

Article

# Magnesium- $\beta$ -Tricalcium Phosphate Composites as a Potential Orthopedic Implant: A Mechanical/Damping/Immersion Perspective

**Gururaj Parande** <sup>1</sup> , **Vyasaraj Manakari** <sup>1</sup> , **Harshit Gupta** <sup>2</sup> and **Manoj Gupta** <sup>1,\*</sup><sup>1</sup> Department of Mechanical Engineering, National University of Singapore, 9 Engineering Drive 1, Singapore 117576, Singapore; gururaj.parande@u.nus.edu (G.P.); mbvyasaraj@u.nus.edu (V.M.)<sup>2</sup> Department of Mechanical Engineering, Indian Institute of Technology (BHU), Varanasi 221005, India; harshit.gupta.mec14@itbhu.ac.in

\* Correspondence: mpegm@nus.edu.sg; Tel.: +65-651-635-8

Received: 6 April 2018; Accepted: 8 May 2018; Published: 11 May 2018



**Abstract:** The design and development of novel magnesium-based materials with suitable alloying elements and bio-ceramic reinforcements can act as a possible solution to the ever-increasing demand of high performance bioresorbable orthopedic implant. In the current study, Mg- $\beta$ -tricalcium phosphate composites are synthesized using the hybrid powder metallurgy technique, followed by hot extrusion. The influence of addition of (0.5, 1, and 1.5) vol %  $\beta$ -tricalcium phosphate on the mechanical, damping, and immersion characteristics of pure magnesium are studied. The addition of  $\beta$ -tricalcium phosphate enhanced the yield strength, ultimate compressive strength, and compressive fracture strain of pure magnesium by about ~34%, ~53%, and ~22%, respectively. Also, Mg 1.5 vol %  $\beta$ -tricalcium phosphate composite exhibited a ~113% enhancement in the damping characteristics when compared to pure magnesium. A superior ~70% reduction in the grain size was observed by the addition of 1.5 vol %  $\beta$ -tricalcium phosphate particles to pure Mg. The response of Mg- $\beta$ -tricalcium phosphate composites is studied under the influence of chloride environment using Hanks' balanced salt solution. The dynamic passivation was realized faster for the composite samples as compared to pure Mg, which resulted in decreased corrosion rates with the addition of  $\beta$ -tricalcium phosphate particles to pure Mg.

**Keywords:** magnesium; tricalcium phosphate; compression; damping; corrosion; powder metallurgy

## 1. Introduction

Bone is a natural composite that is made up of hydroxyapatite and type I collagen [1]. The collagen prevents brittle failure of the bones and makes it elastic whereas hydroxyapatite provides the necessary mechanical strength. In the past few years, noteworthy headways have been made in the research community to keep introducing novel materials that are targeting various biomedical applications to the market. Ceramic and polymer-based biomaterials have superior biocompatibility and bioactivity, thereby finding applications in tissue regeneration and drug delivery [2]. However, insufficient strength and non-biodegradability hinder their application in fixation devices like pins, screws, and plates targeting load-bearing orthopaedic applications. Metal-based biomaterials, like 316 L stainless steel, Ti6Al4V alloy, and Co-Cr biomedical alloy, amongst others, have been long used as commercial orthopaedic implants. Although these implant materials perform the suitable function of assisting in bone remodelling and resorption, a mismatch in elastic modulus between these materials and the bone induces several stress-shielding effects on the bone/implant interface, inducing severe pains to the patient [1]. Either these implants materials are in the human body throughout leading to

apparent toxicity at later stages or may require a secondary surgery to remove the implant adding to the long facing trauma of the patient. In order to solve this issue, the need is to design and develop a biodegradable metal-based orthopaedic implant with superior strengths and optimum degradation rates to serve the purpose of bone remodelling and disintegration into the human body without causing any ill-effects to the patient. Mg, being the lightest structural metal, is also biodegradable, non-toxic, and is abundantly available, and hence it can be a viable solution to be used as orthopedic implant. However, low room temperature ductility and inferior corrosion resistance in biological environments are the reasons why it is not already commercially used in the biomedical sector [3]. However, low room temperature ductility and reduced corrosion resistance in biological environments are the reasons why it is not already commercially used in the biomedical sectors [4–6]. Degradation occurs faster than the bone remodelling process, and hence there is minimum retention of mechanical integrity in the bone chips. There are several ways to retard the degradation rate of Mg, namely alloying, composite technology, and in form of coatings. Although, alloying and coating technology have been effective in improving the biocompatibility and corrosion response of Mg, additional processing steps add to the cost of the eventual product, thus making it less feasible in mass production of implants. Hence, the development of biocompatible materials using cost effective processing techniques is crucial. Therefore, the addition of biocompatible reinforcements using the composite technology to control the degradation rates without adversely affecting the strength properties is the key. Further, Mg has prime importance in the metabolism process, being the second most abundant cation in the human body and it helps in the formation of antibodies maintaining the required wall tension in blood vessels and aids in muscle contraction regulation [7]. Any sort of deficiency in Mg may lead to the change in bone structure, the reduction in osteoblast/osteoclast activity, and may also result in cardiovascular issues, leading to death [8,9].

Calcium (Ca) and Phosphorous (P) are the main minerals in the human bone. Hence, using Ca-P as a reinforcement or coating may be a viable option for enhanced corrosion protection of magnesium-based materials in order to promote bone growth, absorption, and osseointegration [10]. Incorporation of bio-ceramics, like hydroxyapatite (HA) and tricalcium phosphates (TCP), both forms of calcium phosphates, into the Mg matrix seems very promising in the field of bone regeneration. Not only do they exhibit superior biocompatibility and no visible signs of systemic and local toxicity, but also their crystal structure and chemical composition are close to the mineral parts of bone, which may help in tailoring the desired biological properties. Several studies, like the development of Mg-HA composites, AZ91-HA composites, and ZK60-calcium polyphosphate (CPP) composites have been carried out by means of the powder metallurgy technique in the recent past [11–13]. The HA composites reported a decrease in the strength properties although biocompatibility and cell viability of the HA composites were good [14]. The CPP containing composites reported faster pH stabilization, and hence an increased corrosion resistance, however CPP containing composites responded poorly in the tensile mode as compared to the ZK60 base alloy. WE43/HA composites exhibited superior corrosion resistance when immersed in 1% NaCl solution with an appreciable compromise in the compressive strength properties [15]. Hence, superior sintering capability is required for better densification, leading to better strength properties in the Mg bio-ceramic composites. Although, HA possesses superior bioactivity, the better wettability of  $\beta$ -TCP with Mg matrix, and higher dissolution in human physiological environments makes it an ideal candidate for Mg-composite technology targeting orthopaedic implants [16].  $\beta$ -tricalcium phosphate ( $\beta$ -TCP) is an excellent bio-ceramic with superior biocompatibility, chemical stability, and osteointegration behaviour in the body environment, with the resorption rate being better than HA ceramics, thereby finding numerous applications in skeletal and dental prosthetics [14]. Sheng Ying He and coworkers studied the influence of  $\beta$ -TCP nanoparticles on the strength and corrosion properties of the Mg-3Zn-0.8Zr alloy. Both tensile strength and corrosion resistance of the alloy was improved with the addition of  $\beta$ -TCP particles [17]. Liu et al. synthesized Mg-2Zn-0.5Ca-1  $\beta$ -TCP composite using equal channel extrusion processing and noted that the addition of  $\beta$ -TCP improves the mechanical and corrosion properties of Mg-2Zn-0.5Ca.

alloy significantly [18].  $\beta$ -TCP was also investigated as a coating material for surface modification of Mg alloys, with positive results [19]. However, its influence as reinforcement on the mechanical, damping, and immersion response of Mg matrix that is synthesized using solid-state blend-press-sinter powder metallurgy technique is not available in the public domain, which is the novelty of the current study.

## 2. Materials and Methods

### 2.1. Materials and Processing

Magnesium powder of purity  $\geq 98.5\%$  (assay  $> 98.5\%$ , Fe  $< 500$  ppm, substances that are insoluble in HCl  $< 0.005$ ) with a size range of 60–300  $\mu\text{m}$ , supplied by Merck, Germany was used as the base material.  $\beta$ -tricalcium phosphate (reinforcement) with a size range of 0.7–4.6  $\mu\text{m}$  and a purity of  $\geq 96\%$  (assay  $> 96\%$ , Cl  $< 0.05\%$ , Fe  $< 0.1\%$ , K  $< 0.005\%$ , Na  $< 0.005\%$ , Ni  $< 0.005\%$ , Pb  $< 0.005\%$ , Zn  $< 0.005\%$ ) was supplied by Sigma-Aldrich, St. Louis, MO, USA. Pure Mg and Mg 2 vol %  $\beta$ -tricalcium phosphate ( $\beta$ -TCP) composite was synthesized using the powder metallurgy technique, incorporating hybrid microwave sintering [20]. The as-sintered billets were homogenized at 400 °C for 1 h and were then hot extruded at 350 °C to obtain cylindrical rods of 8 mm diameter at an extrusion ratio of 20.25:1. Samples that were cut from the rods were then characterized for physical and mechanical properties.

### 2.2. Material Characterization

#### 2.2.1. Density Measurements

Density measurements were performed on both monolithic and composite samples using the Archimedes principle. Four samples were cut from different parts of the extruded rods and were tested ten times for conformance. The samples were weighed separately in air and water using an A&D ER-182A electronic balance (Bradford, MA, USA) with an accuracy of  $10^{-4}$  g. The theoretical density was calculated using the densities and weight percentages of the constituents by means of the rule of mixtures. From the experimental and theoretical densities, the porosity values of the samples were determined.

#### 2.2.2. Microstructural Characterization

Cylindrical samples were finely polished and etched according to the conventional techniques of metallography to obtain a clear distinction between the grain boundaries with the help of a LEICA-DM 2500M metallographic light microscope (Singapore). Four representative micrographs were analyzed for each composition in order to obtain accurate grain sizes. The OLYMPUS metallographic microscope (Singapore) and JEOL JSM-5800 LV Scanning Electron Microscope (SEM, Kyoto, Japan) was used for the microstructural characterization studies.

X-ray diffraction studies were carried out on extruded samples in the direction along the axis of extrusion. The studies were performed using an automated Shimadzu LAB-XRD-6000 (Cu K $\alpha$ ;  $\lambda = 1.54056 \text{ \AA}$ , Kyoto, Japan) using a scan speed of 2°/min. The studies were conducted to identify the possible formation of any impurities/secondary phases. The XRD analysis was also conducted on the post-corroded samples to identify the corrosion products that were formed.

#### 2.2.3. Damping and Elastic Modulus

Damping characteristics and elastic modulus of the cylindrical samples (7 mm diameter and 60 mm length) were analyzed using the resonant frequency and the damping analyzer (RFDA) equipment from IMCE, Genk, Belgium. Recordings of the vibration signal were obtained in terms of amplitude vs. time. Damping capacity, loss rate, and elastic modulus values for both pure Mg and Mg (0.5, 1.0, and 1.5) vol %  $\beta$ -TCP composite sample were recorded.

## 2.2.4. Mechanical Properties

Microhardness tests were performed on the composite samples using Vickers microhardness tester Matsuzawa MXT 50 (Kyoto, Japan) with an indenter phase angle  $\sim 136^\circ$ ; in conformance with ASTM standard E384-11-1 [21]. Fifteen readings were taken to arrive at an average representative value.

Compression testing in the quasi-static mode was performed on cylindrical samples having 8 mm diameter and 8 mm length, utilizing a fully automated servo-hydraulic mechanical testing machine (Model-MTS 810; in conformance with ASTM test method E9-09, Eden Prairie, MN, USA) at a strain rate  $8.33 \times 10^{-5} \text{ s}^{-1}$  [22]. Four specimens each for both of the compositions were tested to ensure reproducibility. Fracture surface analysis of the samples failed under compression was done using SEM.

## 2.2.5. Immersion Studies

Cylindrical samples of (5 mm diameter and 5 mm length) were immersed for 96 h in Hanks balanced salt solution (HBSS) procured from Lonza Chemicals Pte Ltd. Singapore. The setup was immersed in a water bath that was maintained at  $37^\circ\text{C}$  to simulate the temperature of the human body. The sample dimensions of 5 mm diameter and 5 mm length was used. Solution to sample ratio was maintained at 20 mL:1 cm<sup>2</sup>. The solution was changed every 24 h. Weight loss and pH measurements were measured after every 24 h. A solution containing 20 g CrO<sub>3</sub> and 1.9 g AgNO<sub>3</sub> dissolved in 100 mL of de-ionized water was used for removing the corrosion products. The samples post-corrosion were observed under the SEM in order to gain further information about the nature of corrosion products that were formed.

## 3. Results and Discussion

### 3.1. Density and Porosity

Table 1 shows the density and porosity levels of pure Mg and Mg- $\beta$ -TCP composites. The experimental density of Pure Mg slightly increased with the incorporation of  $\beta$ -TCP, and Mg-1.5 TCP composite exhibited an experimental density value of  $1.7449 \text{ g}\cdot\text{cm}^{-3}$ . The slight increase (0.2%) in the density can be attributed to the fact that there is a density difference between the matrix ( $1.74 \text{ g}\cdot\text{cm}^{-3}$ ) and reinforcement ( $3.14 \text{ g}\cdot\text{cm}^{-3}$ ). Porosity levels marginally increased with the addition of the  $\beta$ -TCP and the highest porosity value of  $\sim 0.28\%$  was observed for the Mg-1.5 TCP composite. The observed porosity is less than 1% porosity, which is an advantage when compared to conventional sintering processes that can achieve only up to  $\sim 95\%$  densification [23]. Microstructural examination of the extruded rod revealed the absence of blowholes, defects and a superior surface finish indicated the suitability of the powder metallurgy technique to generate near dense composites [3].

**Table 1.** Density, porosity, grain size and microhardness measurements of pure Mg and Mg- $\beta$ -tricalcium phosphate ( $\beta$ -TCP) composite.

Material	Theoretical Density ( $\text{g cm}^{-3}$ )	Experimental Density ( $\text{g cm}^{-3}$ )	Porosity (%)	Grain Size ( $\mu\text{m}$ )	Hardness (Hv)
Pure Mg	1.74	$1.7363 \pm 0.002$	0.21	$34 \pm 2$	$46 \pm 3$
Mg-0.5 TCP	1.7412	$1.7371 \pm 0.0147$	0.23	$18 \pm 2$ ( $\downarrow 47\%$ )	$52 \pm 2$ ( $\uparrow 13.04\%$ )
Mg-1.0 TCP	1.7424	$1.7381 \pm 0.0067$	0.24	$13 \pm 1$ ( $\downarrow 61\%$ )	$54 \pm 3$ ( $\uparrow 17.39\%$ )
Mg-1.5 TCP	1.7449	$1.7387 \pm 0.0048$	0.28	$10 \pm 1$ ( $\downarrow 70\%$ )	$54 \pm 1$ ( $\uparrow 17.39\%$ )

### 3.2. Microstructural Characterisation

Table 1 shows the average grain size values of pure Mg and Mg (0.5, 1.0, and 1.5) vol %  $\beta$ -TCP composites. The grain size of pure Mg in as-extruded form was observed to be  $\sim 34 \mu\text{m}$ . The addition of 0.5 vol %  $\beta$ -TCP particles resulted in superior grain refinement of up to  $\sim 18 \mu\text{m}$ , which is  $\sim 47\%$  finer than that of pure Mg. Increased addition of 1.0 and 1.5 vol %  $\beta$ -TCP particles resulted in a further

refinement in the grain size of up to ~13 and ~10  $\mu\text{m}$ . Near equiaxed grain morphology was observed with the addition of  $\beta$ -TCP particles, as observed in Figure 1. This superior grain refinement can be attributed to mainly two aspects namely (a) Particle stimulated nucleation phenomenon that promotes the nucleation of grains, hence restricting the grain growth; (b) the ability of the  $\beta$ -TCP particles to pin the grain boundaries resulting in finer microstructure [24]. As the size of the reinforcement is predominantly in micron length scale, simulated dynamic recrystallization phenomenon can be expected during the extrusion process [25]. Distribution of the  $\beta$ -TCP particle in the Mg matrix is shown in Figure 2. The efficient extrusion process has managed to break down the large  $\beta$ -TCP particles and clusters, leading to a reasonable distribution pattern. Hence, hot extrusion can be considered as a suitable secondary process to promote the near uniform distribution of reinforcement and simultaneously reducing the spatial heterogeneity of the mechanical properties of the Mg-based composites [16]. The superior grain refinement also aids in the strengthening of the composites by means of Hall-Petch mechanism activation.

High wettability of  $\beta$ -TCP particles with the Mg matrix leads to the easy densification under sintering, and hence showing a superior interfacial integrity between the particle and the matrix. The near-uniform distribution of  $\beta$ -TCP throughout the Mg matrix can also be attributed to the suitable primary and secondary processing parameters that are optimized for the primary processing of Mg- $\beta$ -TCP composites. Energy Dispersive Spectroscopy (EDS) analysis of Mg-1.0 TCP composite is also shown in Figure 2. The EDS spectra are studied at the reinforcement (A) and matrix (B) location. The analysis of the matrix reveals predominantly Mg phases with traces of O due to surface oxidation during the processing of the material. The  $\beta$ -TCP particles have settled at the grain boundaries of the composite, hence confirming the grain boundary pinning mechanism that is responsible for grain refinement as quantitatively confirmed by the predominant Ca, O, P peaks in the spectrum. The EDS also confirms the absence of any sign of impurities or secondary phases in the composite.

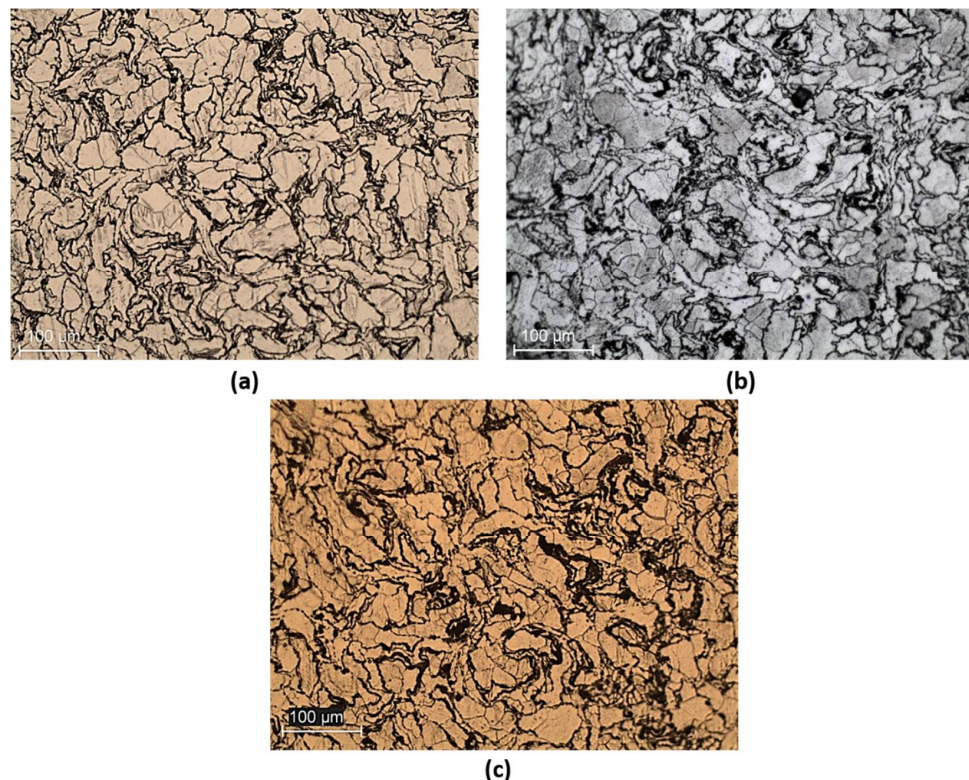


**Figure 1.** Optical micrography images of Mg- $\beta$ -TCP composites: (a) Mg-0.5 TCP; (b) Mg-1.0 TCP; and, (c) Mg-1.5 TCP.

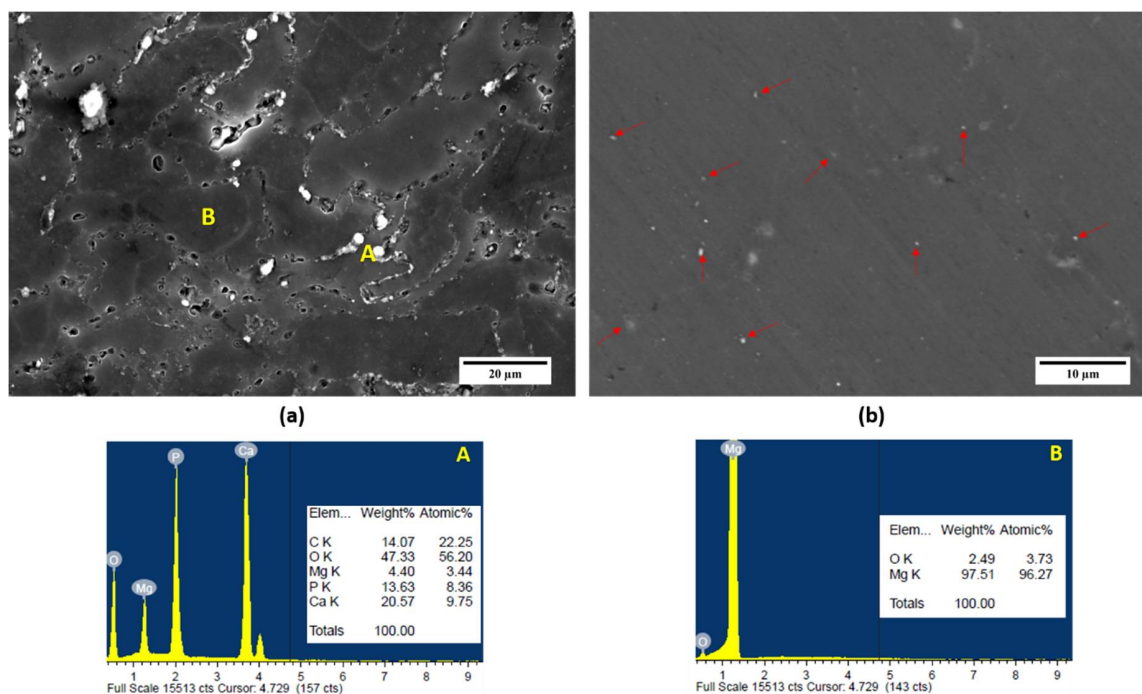


**Figure 2.** (a) Grain boundary pinning mechanism of Mg-1.0 TCP composite; (b)  $\beta$ -TCP particle distribution within the Mg matrix in Mg-1.5 TCP composite. Energy Dispersive Spectroscopy (EDS) analysis of the Mg-1.0 TCP composite at the matrix and reinforcement location.

The X-ray diffraction analysis of the developed composites was performed along the extruded direction and shown in Figure 3. The X-ray diffraction peaks of pure Mg and Mg- $\beta$ -TCP composites reveal mainly Mg peaks. The reinforcement peaks are not visible, as the amount of reinforcement in the Mg matrix is low (<2 vol %), which might go undetected in the X-ray analysis. No MgO peaks, secondary phase, or impurity peaks were observed, which suggests that the surface oxidation during the compaction, sintering, or extrusion process is minimum, and the higher densification of the composite can be realized.

The ratio of the respective intensities to the maximum intensity of the composites ( $I/I_{max}$ ) is also shown in Table 2. The addition of  $\beta$ -TCP to Mg matrix has resulted in a texture randomization with all of the developed composites having dominant intensities corresponding to the pyramidal plane. From Table 2, it can be seen that the initial addition of the reinforcement results in a decrease in the intensity corresponding to the basal plane, which reaches a maximum value with the addition of 1 vol %  $\beta$ -TCP and decreases with further addition up to 1.5 vol %  $\beta$ -TCP. The high  $I/I_{max}$  values corresponding to the basal plane assists in the corrosion protection of the material. The texture modification due to the presence of  $\beta$ -TCP particles may result in a particle stimulated nucleation mechanism, and it assists in systematic recrystallization of randomly oriented grains along the extrusion axis [16].

### 3.3. Microhardness

The results of the microhardness tests that were performed on pure Mg and Mg (0.5, 1.0, and 1.5) vol %  $\beta$ -TCP composite are presented in Table 1. The addition of 0.5 vol %  $\beta$ -TCP particle increased the microhardness of pure Mg (~46 Hv) by ~13% to an average value of ~52 Hv. Further addition of 1.0 and 1.5 vol %  $\beta$ -TCP particles show minimal enhancement in the microhardness of the composite. The microhardness results of Mg 1.5 vol %  $\beta$ -TCP composite reveal the improvement of ~17% when compared to pure Mg, hereby indicating the increased resistance to indentation. This increase in the hardness value can be attributed to the nearly uniform distribution of  $\beta$ -TCP particles throughout the

Mg matrix (Figure 2) and the reduced grain size (Table 1) of the Mg- $\beta$ -TCP composite, leading to the increased resistance to localized plastic deformation [3].

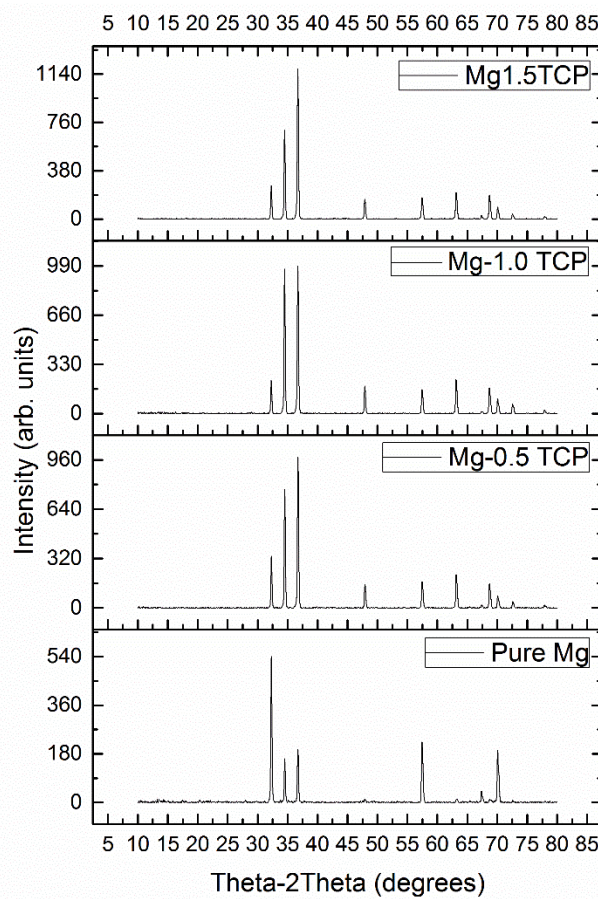


**Figure 3.** X-ray diffractograms of pure magnesium and Mg (0.5, 1.0, and 1.5) vol %  $\beta$ -TCP composites along the longitudinal direction.

**Table 2.** The ratio of intensities w.r.t the maximum intensity for the as-extruded Mg- $\beta$ -TCP composites.

Material	Plane	$I/I_{max}$
Pure Mg	Prismatic	1.00
	Basal	0.29
	Pyramidal	0.36
Mg-0.5 TCP	Prismatic	0.34
	Basal	0.76
	Pyramidal	1.00
Mg-1.0 TCP	Prismatic	0.22
	Basal	0.98
	Pyramidal	1.00
Mg-1.5 TCP	Prismatic	0.23
	Basal	0.58
	Pyramidal	1.00

### 3.4. Damping Characteristics and Elastic Modulus

Figure 4 and Table 3 shows the damping characteristics of pure Mg and Mg (0.5, 1.0, and 1.5) vol %  $\beta$ -TCP composites. The time taken for pure Mg to absorb vibration is  $\sim 0.37$  s. The gradual addition

of  $\beta$ -TCP particles resulted in a linear decrease in the time that is taken by the material to absorb vibration with Mg-1.5 TCP absorbing the vibration as quick as  $\sim 0.28$  s. Table 3 discusses the damping loss rate, damping capacities, and elastic modulus of the composite samples. The damping loss rate ( $L$ ) and damping capacity ( $Q^{-1}$ ) of pure Mg enhanced with the increased presence of  $\beta$ -TCP with Mg-1.5 TCP composite exhibiting the best value of  $\sim 17.7$  and  $\sim 7.59 \times 10^{-4}$ , respectively. The enhancement in damping loss rate and damping capacity for Mg-1.5 TCP composite was  $\sim 109\%$  and  $\sim 15.7\%$  when compared to that of pure Mg, respectively.

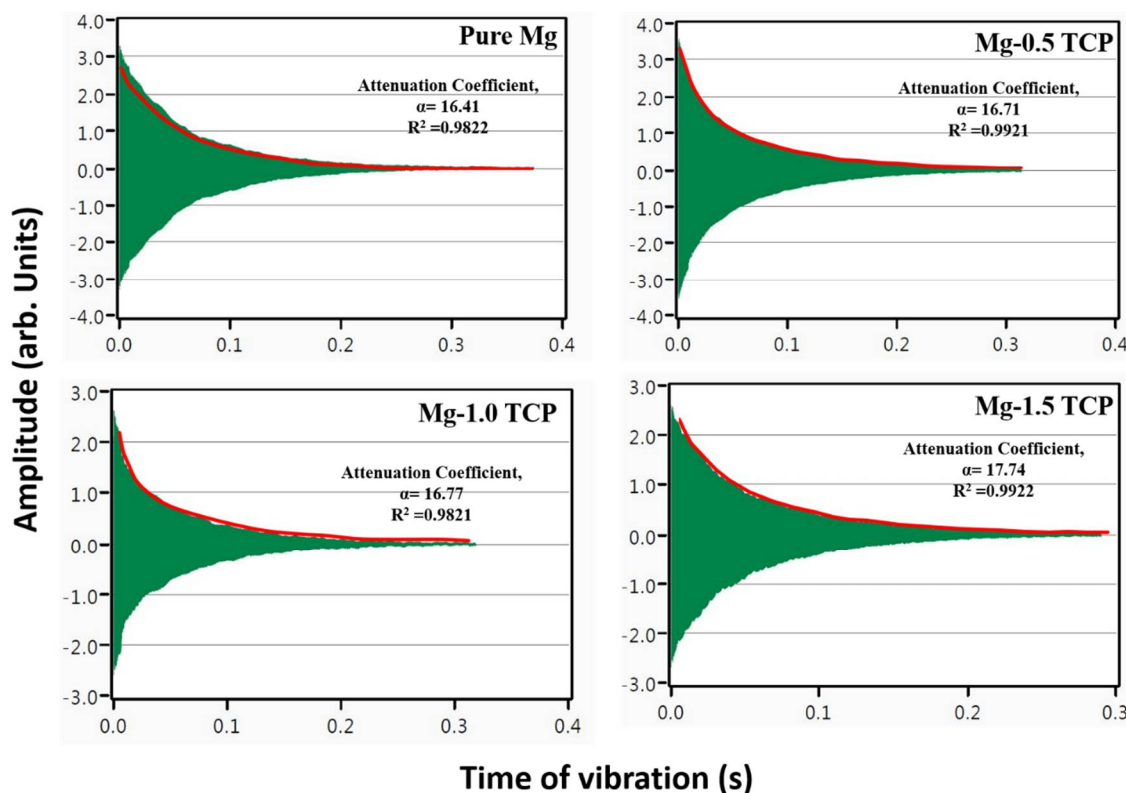


**Figure 4.** Damping characteristics of pure magnesium and Mg (0.5, 1.0, and 1.5) vol %  $\beta$ -TCP composites.

**Table 3.** Damping characteristics of pure Mg and Mg (0.5, 1.0, and 1.5) vol %  $\beta$ -TCP composites.

Material	Damping Loss Rate ( $L$ )	Damping Capacity ( $Q^{-1}$ ) ( $\times 10^{-4}$ )	Elastic Modulus (GPa)
Pure Mg	$8.3 \pm 0.2$	$6.56 \pm 0.2$	$44.7 \pm 0.2$
Mg-0.5TCP	$15.7 \pm 0.9$ ( $\uparrow 89\%$ )	$6.94 \pm 0.2$ ( $\uparrow 5.7\%$ )	$43.7 \pm 0.4$
Mg-1.0 TCP	$17.4 \pm 0.7$ ( $\uparrow 109\%$ )	$6.96 \pm 0.3$ ( $\uparrow 6.0\%$ )	$43.5 \pm 0.08$
Mg-1.5 TCP	$17.7 \pm 0.5$ ( $\uparrow 113\%$ )	$7.59 \pm 0.2$ ( $\uparrow 15.7\%$ )	$43.7 \pm 0.6$

The superior enhancement in the damping characteristics of pure Mg with the addition of  $\beta$ -TCP may be attributed to the contribution of several damping mechanisms, namely (a) damping behavior at particle/matrix interface; (b) dislocation density owing to Mg and TCP thermal mismatch; and, (c) bulk texture modifications [26]. Other properties, like porosities and micro-defects, also affect the damping response of magnesium. However, the effect of this phenomenon on the damping characteristics of the material is a combined effect of their interactions and is not monotonically related to a particular mechanism. Attenuation coefficient calculations provide interesting insights into the qualitative understanding of the damping mechanisms of Mg-based materials. The amplitude versus time plots are shown in Figure 4. In theory, with the passage of time, the amplitude of free vibration decreases in Mg-based materials. Attenuation coefficient quantifies this difference and it is represented

as the steepness of the curve in the amplitude-time plot. The composite samples excited during the study vibrate at their natural resonant frequency before attaining equilibrium. This amplitude of the dampening vibration ( $A(t)$ ) can be expressed as Equation (1).

$$A(t) = A_0 \cdot \exp[-at] + C \quad (1)$$

where,  $A_0$  is the amplitude at  $t = 0$ ,  $a$  is the apparent attenuation coefficient,  $t$  is the time after the removal of impulse, and  $C$  is the fitting coefficient.

The attenuation coefficients of pure Mg increased with the presence of  $\beta$ -TCP particles. The attenuation coefficients of Mg-0.5 TCP and Mg-1.0 TCP are very similar to the attenuation coefficient of pure Mg. The addition of 1.5 vol %  $\beta$ -TCP particle has further enhanced the attenuation coefficient. The trend that was observed in this case is very similar to the  $Q^{-1}$  values of the composites with respect to pure Mg. This behavior is majorly dependent on the size, shape, density, and elastic modulus of the specimen that was used for measurement. The change in vibrational amplitude and resonant frequency influenced the overall improvement of the composite material when compared to that of pure Mg.

In case of Mg-based materials, dislocation pinning that is caused by increased dislocation density is favorable for achieving superior damping characteristics. This increased dislocation density owing to the mismatch in the coefficient of thermal expansions of the Mg matrix and the ceramic reinforcement results in a high volume of energy dissipation agents. This mismatch can also cause several plastic deformation zones at the matrix/reinforcement interface. The higher the plastic deformation zones and strain amplitudes, the higher the damping capacities that can be realized using the composite technology. In order to obtain high volume of plastic deformation zones, high amount of reinforcement is desirable. However, in the current case the addition of reinforcement in micron-length scale is <2 vol %. Hence, the damping capacities of the composites are close to each other [27,28].

Elastic modulus and damping capacity are two crucial properties in order to qualify any material as an orthopedic implant [3]. Currently used biomaterials, like Ti6Al4V (113 GPa), 316 L stainless steel (193 GPa), and Co-Cr alloy (230 GPa), amongst others, have high elastic modulus when compared to that of the natural bone (2–20 GPa). This huge elastic modulus mismatch might lead to stress shielding effects, hence decreasing the stimulated bone growth resulting in the failure of the implant [29]. Mg- $\beta$ -TCP composites display elastic modulus (~45 GPa) that is closer to that of the natural bone when compared to the commercially available implants, and hence could be highly effective in decreasing the effect of stress shielding. Superior damping capacity values assists in the mitigation of the vibrations caused by the patient movement by suppressing the developed stresses at the implant-bone interface to result in superior osseointegration [30].

### 3.5. Immersion Studies

The pH, weight change, and corrosion rate measurements with respect to the time of immersion of Mg and Mg- $\beta$ -TCP composites are shown in Figure 5 and Table 4. The pH of Mg showed a sudden increase post 24 h of immersion. Further immersion of up to 96 h led to a relatively slow and uniform increase in the pH, as shown in Figure 5a. The addition of  $\beta$ -TCP particles to the Mg matrix resulted in a lower pH reading at the end of every 24 h as compared to pure Mg. The sudden increase in the pH during the initial stage is characteristic for Mg-based materials due to high anodic  $Mg^{2+}$  dissolution [31]. However, post 24 h, the stabilization of pH is observed to be quicker for the composites when compared to pure Mg. Lower pH values and the corrosion rate values in the case of composites suggest that the amount of  $Mg^{2+}$  dissolution is lesser for the Mg- $\beta$ -TCP composites when compared to pure Mg. It is well known in Mg-biomaterial community that the maximum hydrogen evolution happens in the first 12–24 h of immersion in salt solutions and biofluids [32]. Hence, the presence of  $\beta$ -TCP particle in the magnesium matrix helps in faster pH stabilization, thereby a controlled degradation can be achieved.

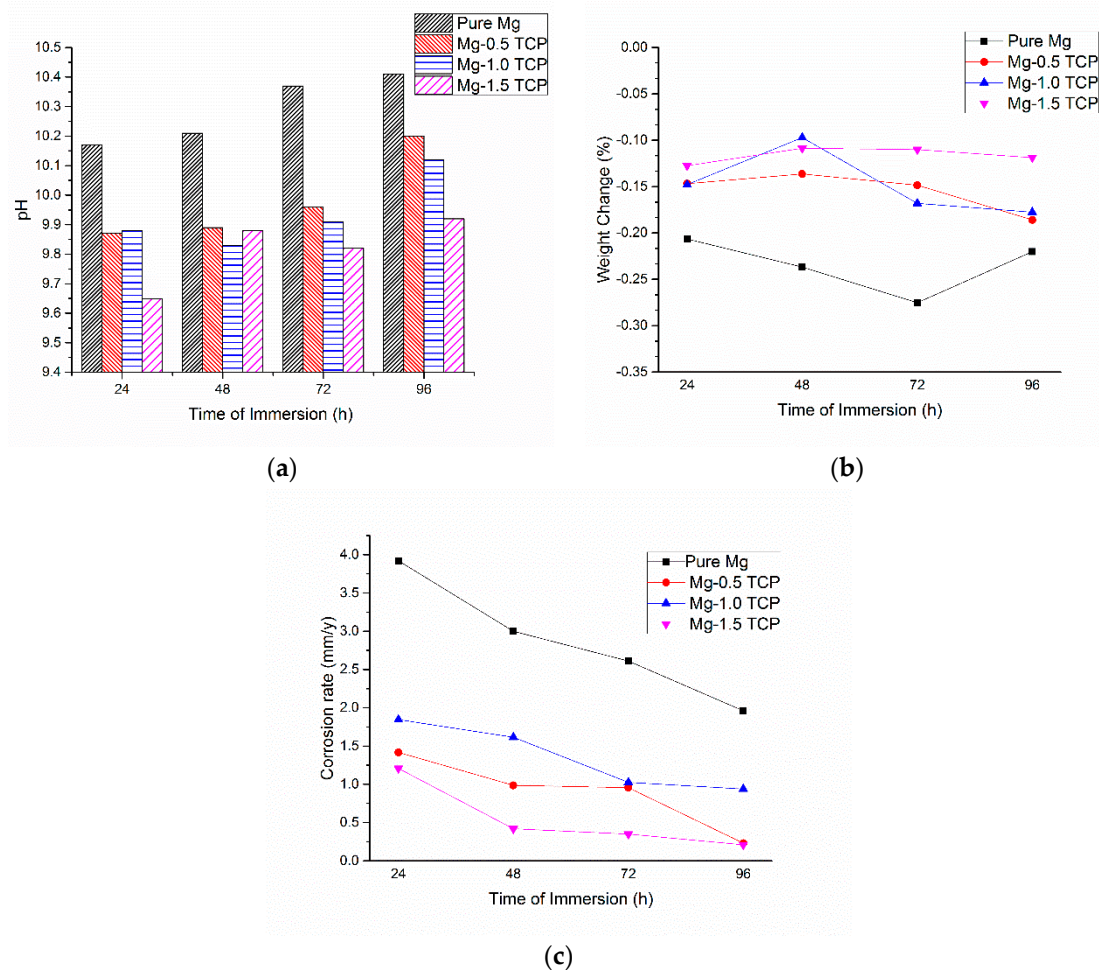


**Figure 5.** (a) pH vs. Time of immersion; (b) Weight change (%) vs. Time of immersion (h); and, (c) Corrosion rate vs. Time of immersion (h).

**Table 4.** Corrosion rate and pH measurements of the composite samples after 96 h of Hanks balanced salt solution (HBSS) immersion. A comparison is made with existing Mg-based alloys.

Material	Corrosion Rate (mm/Year)	pH
Pure Mg	1.95	10.41
Mg-0.5 TCP	0.23	10.23
Mg-1.0 TCP	0.92	10.11
Mg-1.5 TCP	0.21	9.92
Pure Mg [32]	2.08	
Mg1Ca [32]	3.16	
Mg1Ca1Zn [32]	2.13	
Mg1Ca3Zn [32]	2.92	
Mg5Zn [33]	2.25	-
Mg5Zn0.2Sr [33]	1.75	
Mg3Sr [32]	0.75	
ZE41 [34]	2.04	
AZ91 [34]	3.56	

From Figure 5b, it can be observed that the weight loss of the material due to immersion is gradually increasing for pure Mg with an increased time of immersion of up to 72 h. In the case of Mg- $\beta$ -TCP composites, the weight changes as compared to pure Mg are observed to be lesser in all

of the cases. In the case of Mg-1.5 TCP composite, the weight change is almost constant through the period, which is desirable in order to achieve a uniform dissolution of a material in vitro and in vivo conditions. Mg-0.5 TCP and Mg-1.0 TCP composites also exhibit near uniform weight loss with the increase in immersion time. Figure 5c represents the change in corrosion rate (mm/year) with the time of immersion, and is calculated by Equation (2) [35].

$$CR = \frac{(K \times W)}{(A \times T \times D)} \quad (2)$$

where, time conversion coefficient,  $K = 8.76 \times 10^4$ ,  $W$  is the change in weight pre and post-immersion (g),  $A$  is the surface area of the cylinder exposed to the immersing medium ( $\text{cm}^2$ ),  $T$  is the time of immersion (h), and  $D$  is the experimental density of the material ( $\text{g}\cdot\text{cm}^{-3}$ ).

The corrosion rate is a factor of the change in weight, surface area exposed to immersion liquid, and the time of immersion. The corrosion rates of the composites are observed to be lesser than that of pure Mg with Mg-1.5 TCP composite exhibiting the least corrosion rates for all of the conditions. The corrosion rate values owing to the weight loss of the composites mainly depend on two factors, namely (a) an initial period of incubation from the protective layer formation and breaking and (b) subsequent increase in the volume of hydrogen evolved with respect to the immersion time [34]. The corrosion rates of the composites in the current study are compared to the corrosion rates of several potential Mg-based orthopedic materials in HBSS. The corrosion rate of Mg-0.5 TCP composite (Table 4) is either better or as good as potential Mg-based alloys that are suited for orthopedic applications [32]. This justifies the suitability of Mg- $\beta$ -TCP composite as a potential candidate for orthopedic applications and encourages the scientific community to further the research in this domain.

The corrosion of pure Mg and Mg- $\beta$ -TCP composites are mainly governed by the way that Mg responds in aqueous environments. The Mg samples once immersed in the HBSS leads to severe anodic dissolution during the initial immersion, which leads to a sudden increase in the pH of the developed composites. However, post-initial anodic dissolution,  $Mg^{2+}$  from the anodic metal will react with  $OH^-$  in the HBSS to form a protective porous  $Mg(OH)_2$  layer [4,31]. The formation of this layer will thereby protect the material by covering the surface and discouraging attack from the immersing medium. This formation of  $Mg(OH)_2$  layer might stabilize the corrosion rate and the pH values of the developed composites that are observed in the current study as well. The pH and corrosion rate of the composites stabilized around a time range from 24–72 h. However, the immersing medium will slowly permeate into the sample, thereby increasing the weight loss of the sample. It is common knowledge that the corrosion resistance of Mg in chloride environments is low and the presence of  $Cl^-$  ions in Hank's solution promotes the corrosion rate by forming more soluble  $MgCl_2$ , thereby increasing the concentration of  $OH^-$  ions in the solution and hence rupturing the protective hydroxide layer [36]. The  $Cl^-$  attack on the sample leads to the pitting corrosion of the material, which is the most commonly seen mechanism for Mg-based materials. Post this behaviour, a dynamic stabilization is observed in the pH and corrosion rate values and a near uniform dissolution of the material is observed. However, with the passage of time, these reactions might continue to have a deeper impact along the matrix/particle interface, allows for the swelling of the composites due to electrolyte penetration, leading to the eventual failure of the composite [37]. Figure 6 shows the optical micrographs of the samples under immersion. The formation of corroded pits is very evident with pure Mg and the number of corroded pits that were formed on the composites samples are much lesser than that of pure Mg.

By theory, in addition to pitting corrosion, corrosion at the grain boundaries is a major form of corrosion in the Mg-based materials [4,5,38]. However, due to the high chemical activity of Mg in chloride environments, realizing a near uniform corrosion rate is ideal. Hence, altering Mg microstructurally can assist in realizing this. In the current study, the refinement in the grain size of pure Mg with the addition of  $\beta$ -TCP particles strongly aids in the corrosion protection of Mg. The increased number of grain boundaries due to their higher energies and chemical activities increase

the surface reactivity, realising the faster formation of the protective layer by relieving the extent of localized corrosion [5,39]. The reduction of the number of cathodic sites can also enhance the corrosion resistance, owing to the dissolution of impurities at the grain boundaries [40]. Further, the absence of secondary phases/impurities in the material, which might serve as a stress concentration sites leading to stress corrosion cracking, also supports the enhancement of the corrosion protection. In addition to the superior grain refinement, the high intensities corresponding to the basal plane of the Mg- $\beta$ -TCP composites also assists in increasing the corrosion resistance of the material [40]. The lower porosities that were observed for the composite samples can also assist in mitigating the effect of corrosion. The cumulative effect of lower grain size coupled with higher basal intensities of the composites is responsible for the lower corrosion rates of the composites when compared to that of pure Mg [40]. Further, the presence of Fe impurity (<500 ppm) in the magnesium powder might be responsible for a high corrosion rate value of pure Mg. The addition of  $\beta$ -TCP tends to override the effect of the Fe impurity, as observed by the lower corrosion rates of the composites. Although, the presence of the Fe impurity cannot be confirmed by the XRD and EDS analysis of the composites, its effect on the corrosion rate could still be acknowledged to be significant. In order to understand the effect of any alloying element/secondary reinforcement on the corrosion performance of pure Mg, ultra-pure Mg must be used so that the Fe content can be restricted to <45 ppm in the extruded form and the direct effect of the secondary reinforcement could be more accurately discussed [9].

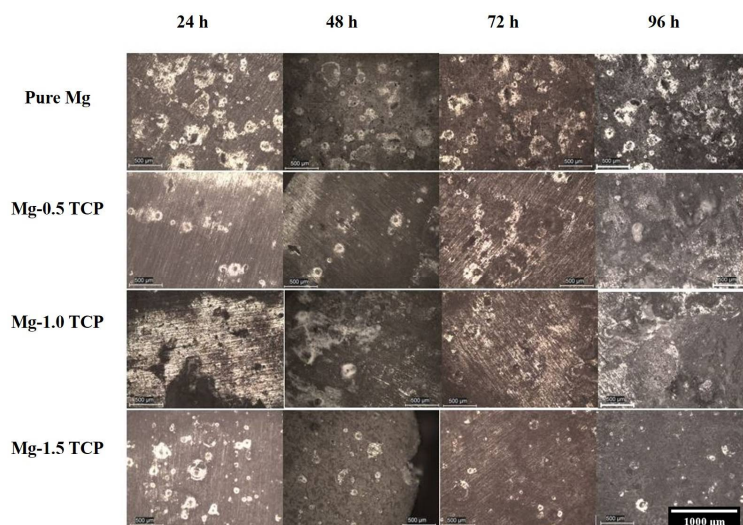


**Figure 6.** Optical micrographs of pure magnesium and Mg (0.5, 1.0, and 1.5) vol %  $\beta$ -TCP composites after 24, 48, 72, and 96 h of immersion.

The SEM analysis of the corroded surface of the Mg-1.0 TCP composite samples post 96 h of immersion is shown in Figure 7. The removal of the composite samples from the immersive medium and drying in the air before undergoing SEM observation shrinks the protective film on the surface, owing to dehydration [41]. This leads to severe cracking on the sample surface with two types of layers namely quasi-adherent layer and cracked layer being formed [4]. Several uneven corrosion pits with varying sizes and cracks were observed throughout the sample surface [41]. Apart from this, many tiny cracks were observed through the sample surface. Figure 8 shows the XRD analysis of the samples post-corrosion. The XRD analysis of the composites reveals the presence of corrosion products like  $Mg(OH)_2$ ,  $(Ca_2Mg)_3(PO_4)_2$  and Hydroxyapatite (HA). These corrosion products fill these corrosion pits, forming a protective layer and hence delaying the corrosion attack to the surface [36]. Hence, the behaviour of the Mg- $\beta$ -TCP composites can be observed to be better than that of pure Mg. The corrosion product layer that was formed in pure Mg destabilizes faster, leading to the HBSS to penetrate the matrix influencing the corrosion along the grain boundaries and the impurities, if any.

The HA corrosion products can encourage the formation of apatite layer at the implant/bone interface, which therefore assists in the osteoclast activity and resulting in faster bone formation, as compared to monolithic Mg [42].

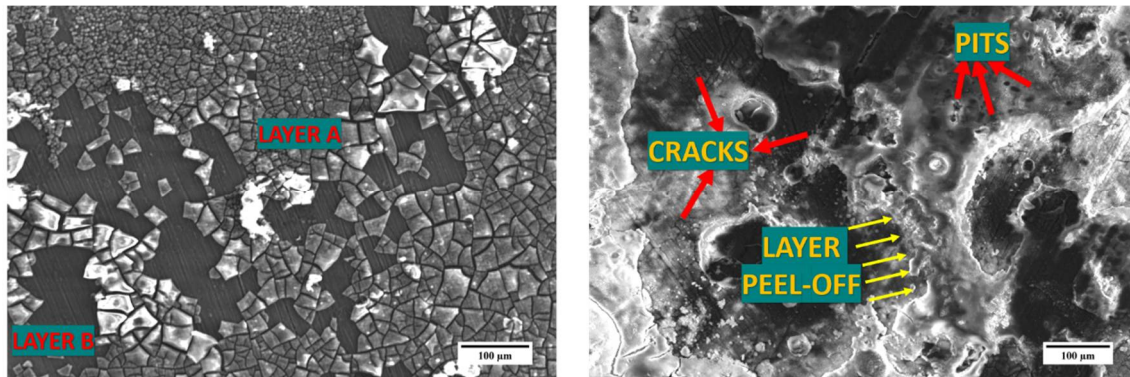


**Figure 7.** Scanning Electron Microscope (SEM) analysis of Mg-1.0 TCP composite post 96 h of Hanks balanced salt solution (HBSS) immersion.

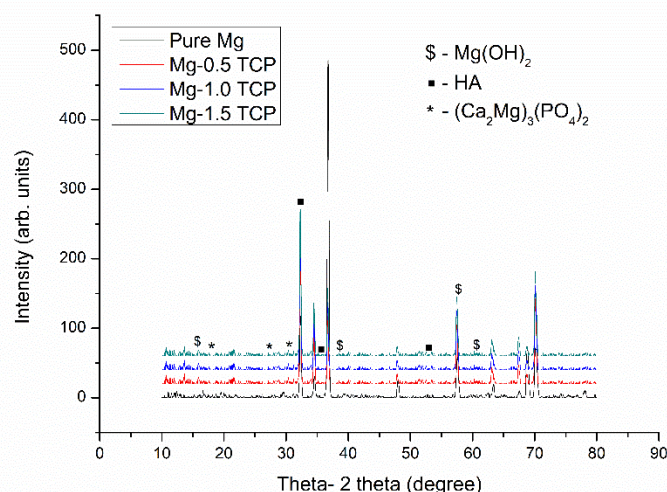


**Figure 8.** X-ray diffraction studies on the corroded samples post 96 h immersion in HBSS.

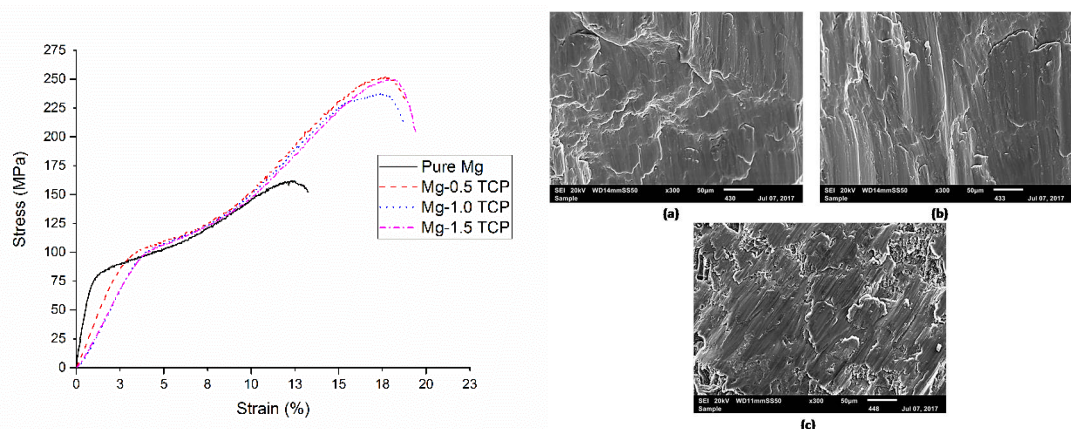
### 3.6. Compression Properties

Table 5 and Figure 9 shows the compressive properties and the stress-strain behavior of the composites. Addition of  $\beta$ -TCP enhances the overall compressive properties of pure Mg. The compressive yield strength (0.2% CYS) of Mg (0.5, 1.0 and 1.5) vol % TCP was observed to be ~92 MPa, ~96 MPa and ~103 MPa, respectively, which is ~19%, ~24%, and ~34% greater than that of pure Mg (~77 MPa). The addition of 0.5 vol % TCP increases the ultimate compressive strength (UCS) to the value of ~258 MPa, which is a ~65% enhancement when compared to pure Mg (~156 MPa). Further addition of TCP particles resulted in a decrease in the UCS values, with both Mg-1.0 TCP and Mg-1.5 TCP composites remaining lower than that of Mg-0.5 TCP. However, the UCS values of the composites still exhibited a ~42% and ~53% enhancement, respectively, with respect to pure Mg. The maximum fracture strain and energy absorbed under compressive loading was observed for Mg-1.5 vol % TCP composite with ~19.3% and ~29.2 MJ/m<sup>3</sup>, which is ~22% and ~64% greater than that of pure Mg.

**Table 5.** Room temperature compressive testing results.

Material	0.2 CYS (MPa)	UCS (MPa)	Fracture Strain (%)	Energy Absorbed (MJ/m <sup>3</sup> )
Pure Mg	77 ± 5	156 ± 7	15.8 ± 0.3	17.7 ± 0.7
Mg-0.5 TCP	92 ± 1 ( $\uparrow$ 19%)	258 ± 4 ( $\uparrow$ 65%)	18.5 ± 0.6 ( $\uparrow$ 17%)	28.3 ± 1.3 ( $\uparrow$ 59%)
Mg-1.0 TCP	96 ± 2 ( $\uparrow$ 24%)	223 ± 7 ( $\uparrow$ 42%)	17.2 ± 0.7 ( $\uparrow$ 9%)	23.2 ± 2.9 ( $\uparrow$ 31%)
Mg-1.5 TCP	103 ± 7 ( $\uparrow$ 34%)	240 ± 7 ( $\uparrow$ 53%)	19.3 ± 0.5 ( $\uparrow$ 22%)	29.2 ± 2.4 ( $\uparrow$ 64%)

The significant increase in the strengths of Mg- $\beta$ -TCP composite may be due to: (a) superior grain refinement (Table 1), leading to activation of Hall-Petch strengthening mechanism [3]; (b) uniformly distributed  $\beta$ -TCP particles that are acting as an obstacle to dislocation movement through the Orowan strengthening mechanism [16]; (c) forest strengthening of the composite owing to the thermal coefficient mismatch between the matrix (Mg) and the ceramic reinforcement ( $\beta$ -TCP); (d) combined effects of texture randomization and deformation twinning creating additional barriers to the crack path leading to enhanced compressive strengths [43]; and, (e) effective load transfer from the ductile matrix to the brittle ceramic, owing to the good interface with each other. Due to high interfacial integrity between the matrix and the reinforcement, the crack propagates preferentially through the soft matrix phase under compressive loading. When the crack encounters the soft matrix, the matrix deforms, thereby creating a bridging mechanism, leading to crack closure and resistance to crack initiation and growth [36,44]. Hence, the sample fracture under compression is mainly driven by the matrix deformation. The fracture strain of the composite samples remained as marginally superior to that of pure Mg, unlike in the case of submicron and micron size ceramic particles where it is adversely affected. Figure 9 shows the fractured surface analysis of the composite samples. The fractured surfaces show typical shear band formation, which corroborates the fact that the composite fracture is mainly matrix driven.



**Figure 9.** Compressive stress-strain relationship and fractured surface behavior of Mg ((a) 0.5, (b) 1.0, and (c) 1.5 vol %  $\beta$ -TCP composites.

The cumulative effect of enhanced damping, compression, and corrosion properties is key to qualify a certain material to be a potential orthopaedic implant. In addition to the mitigation of stress-shielding effects and the bioresorbable nature of magnesium, enhanced structural properties are also equally important when considering that Mg-based implants and stents may witness a 15–20% decrease in strength and ductility when being immersed in a physiological environment [45]. With the bone remodelling process taking 10–12 weeks for an average human being, incorporating novel biocompatible reinforcements in the magnesium matrix that can protect pure Mg from expedited degradation and simultaneously perform the task of load-bearing. Further, to understand and to

critically evaluate the possibility of using Mg- $\beta$ -TCP composites in orthopaedic applications, in vivo immersion and cytotoxicity tests must be conducted.

#### 4. Conclusions

- Near dense Mg- $\beta$ -TCP composites were successfully synthesized with blend-press-sinter powder metallurgy technique with a porosity of less than 1%.
- The microhardness of pure Mg increased due to the presence of  $\beta$ -TCP particles with ~17.39% enhancement realized in the case of Mg-1.5 TCP composite.
- Mg-1.5 TCP composite exhibited a compressive yield strength, ultimate compressive strength, compressive fracture strain, and total energy absorbed under compression loading of ~103 MPa ( $\uparrow\sim 34\%$ ), ~240 MPa ( $\uparrow\sim 53\%$ ), ~19.3% ( $\uparrow\sim 22\%$ ), and ~29.2 MJ/m<sup>3</sup> ( $\uparrow\sim 64\%$ ), respectively. The enhancements with respect to the base pure Mg are significant in all of the cases.
- The damping response of pure Mg enhanced with the addition of  $\beta$ -TCP particles, with Mg-1.5 TCP composite exhibiting the best damping capacity (~15.7% increase as compared to pure Mg) and damping loss rate (~113% increase compared to pure Mg) values.
- The presence of  $\beta$ -TCP particles assisted in the corrosion protection of pure Mg. The pH values stabilized earlier for the composites as compared to pure Mg and displayed lower corrosion rate values, which a superior ~9 times protection displayed by the Mg-1.5 TCP composite as compared to pure Mg.

**Author Contributions:** M.G. and G.P. proposed the original project and supervised the investigation. H.G. and G.P. performed the experiments. G.P., V.M. and H.G. analyzed the data and wrote the paper with assistance from all authors. All authors contributed to the discussions in the manuscript.

**Conflicts of Interest:** The authors declare no conflict of interest.

#### References

1. Kuśnirczyk, K.; Basista, M. Recent advances in research on magnesium alloys and magnesium–calcium phosphate composites as biodegradable implant materials. *J. Biomater. Appl.* **2017**, *31*, 878–900. [[CrossRef](#)] [[PubMed](#)]
2. Boccaccini, A.R.; Ma, P.X. *Tissue Engineering Using Ceramics and Polymers*; Elsevier: Amsterdam, The Netherlands, 2014.
3. Parande, G.; Manakari, V.; Meenashisundaram, G.K.; Gupta, M. Enhancing the hardness/compression/damping response of magnesium by reinforcing with biocompatible silica nanoparticulates. *Int. J. Mater. Res.* **2016**, *107*, 1091–1099. [[CrossRef](#)]
4. Song, G.L.; Atrens, A. Corrosion mechanisms of magnesium alloys. *Adv. Eng. Mater.* **1999**, *1*, 11–33. [[CrossRef](#)]
5. Atrens, A.; Song, G.-L.; Liu, M.; Shi, Z.; Cao, F.; Dargusch, M.S. Review of recent developments in the field of magnesium corrosion. *Adv. Eng. Mater.* **2015**, *17*, 400–453. [[CrossRef](#)]
6. Atrens, A.; Song, G.-L.; Cao, F.; Shi, Z.; Bowen, P.K. Advances in mg corrosion and research suggestions. *J. Mates. Alloys* **2013**, *1*, 177–200. [[CrossRef](#)]
7. Tan, L.; Yu, X.; Wan, P.; Yang, K. Biodegradable materials for bone repairs: A review. *J. Mater. Sci. Technol.* **2013**, *29*, 503–513. [[CrossRef](#)]
8. Witte, F. The history of biodegradable magnesium implants: A review. *Acta Biomater.* **2010**, *6*, 1680–1692. [[CrossRef](#)] [[PubMed](#)]
9. Atrens, A.; Liu, M.; Abidin, N.I.Z. Corrosion mechanism applicable to biodegradable magnesium implants. *Mater. Sci. Eng. B* **2011**, *176*, 1609–1636. [[CrossRef](#)]
10. Lu, Y.; Tan, L.; Xiang, H.; Zhang, B.; Yang, K.; Li, Y. Fabrication and characterization of Ca–Mg–P containing coating on pure magnesium. *J. Mater. Sci. Technol.* **2012**, *28*, 636–641. [[CrossRef](#)]
11. Witte, F.; Feyerabend, F.; Maier, P.; Fischer, J.; Störmer, M.; Blawert, C.; Dietzel, W.; Hort, N. Biodegradable magnesium–hydroxyapatite metal matrix composites. *Biomaterials* **2007**, *28*, 2163–2174. [[CrossRef](#)] [[PubMed](#)]

12. Feng, A.; Han, Y. The microstructure, mechanical and corrosion properties of calcium polyphosphate reinforced ZK60A magnesium alloy composites. *J. Alloys Compd.* **2010**, *504*, 585–593. [[CrossRef](#)]
13. Gu, X.; Zhou, W.; Zheng, Y.; Dong, L.; Xi, Y.; Chai, D. Microstructure, mechanical property, bio-corrosion and cytotoxicity evaluations of Mg/Ha composites. *Mater. Sci. Eng. C* **2010**, *30*, 827–832. [[CrossRef](#)]
14. Koepp, H.E.; Schorlemmer, S.; Kessler, S.; Brenner, R.E.; Claes, L.; Günther, K.P.; Ignatius, A.A. Biocompatibility and osseointegration of  $\beta$ -TCP: Histomorphological and biomechanical studies in a weight-bearing sheep model. *J. Biomed. Mater. Res. Part B* **2004**, *70*, 209–217. [[CrossRef](#)] [[PubMed](#)]
15. Dieringa, H.; Fuskova, L.; Fechner, D.; Blawert, C. Mechanical and corrosion behaviour of a hydroxyapatite reinforced magnesium alloy WE43. In Proceedings of the 17th International Conference on Composite Materials, ICCM, Edinburgh, UK, 27–31 July 2009.
16. Yan, Y.; Kang, Y.; Li, D.; Yu, K.; Xiao, T.; Deng, Y.; Dai, H.; Dai, Y.; Xiong, H.; Fang, H. Improvement of the mechanical properties and corrosion resistance of biodegradable  $\beta$ -Ca<sub>3</sub>(PO<sub>4</sub>)<sub>2</sub>/Mg-Zn composites prepared by powder metallurgy: The adding  $\beta$ -Ca<sub>3</sub>(PO<sub>4</sub>)<sub>2</sub>, hot extrusion and aging treatment. *Mater. Sci. Eng. C* **2017**, *74*, 582–596. [[CrossRef](#)] [[PubMed](#)]
17. He, S.-Y.; Sun, Y.; Chen, M.-F.; Liu, D.-B.; Ye, X.-Y. Microstructure and properties of biodegradable  $\beta$ -TCP reinforced Mg-Zn-Zr composites. *Trans. Nonferr. Met. Soc. China* **2011**, *21*, 814–819. [[CrossRef](#)]
18. Liu, D.B.; Huang, Y.; Prangnell, P.B. Microstructure and performance of a biodegradable Mg–1Ca–2Zn–1TCP composite fabricated by combined solidification and deformation processing. *MatL* **2012**, *82*, 7–9. [[CrossRef](#)]
19. Famery, R.; Richard, N.; Boch, P. Preparation of  $\alpha$ - and  $\beta$ -tricalcium phosphate ceramics, with and without magnesium addition. *Ceram. Int.* **1994**, *20*, 327–336. [[CrossRef](#)]
20. Matli, P.R.; Ubaid, F.; Shakoor, R.A.; Parande, G.; Manakari, V.; Yusuf, M.; Mohamed, A.M.A.; Gupta, M. Improved properties of Al–Si<sub>3</sub>N<sub>4</sub> nanocomposites fabricated through a microwave sintering and hot extrusion process. *RSC Adv.* **2017**, *7*, 34401–34410. [[CrossRef](#)]
21. ASTM Standard. E384, *Standard Test Method for Microindentation Hardness of Materials*; ASTM International: West Conshohocken, PA, USA, 2000.
22. ASTM Standard. E9-09. *Standard Test Methods of Compression Testing of Metallic Materials at Room Temperature*; ASTM International: West Conshohocken, PA, USA, 2009.
23. Wong, W.; Gupta, M. Using microwave energy to synthesize light weight/energy saving magnesium based materials: A review. *Technologies* **2015**, *3*, 1–18. [[CrossRef](#)]
24. Parande, G.; Manakari, V.; Meenashisundaram, G.K.; Gupta, M. Enhancing the tensile and ignition response of monolithic magnesium by reinforcing with silica nanoparticulates. *J. Mater. Res.* **2017**, *32*, 2169–2178. [[CrossRef](#)]
25. Wang, X.; Wu, K.; Zhang, H.; Huang, W.; Chang, H.; Gan, W.; Zheng, M.; Peng, D. Effect of hot extrusion on the microstructure of a particulate reinforced magnesium matrix composite. *Mater. Sci. Eng. A* **2007**, *465*, 78–84. [[CrossRef](#)]
26. Kujur, M.S.; Mallick, A.; Manakari, V.; Parande, G.; Tun, K.S.; Gupta, M. Significantly enhancing the ignition/compression/damping response of monolithic magnesium by addition of SM<sub>2</sub>O<sub>3</sub> nanoparticles. *Metals* **2017**, *7*, 357. [[CrossRef](#)]
27. Anilchandra, A.R.; Surappa, M.K. Microstructure and damping behaviour of consolidated magnesium chips. *Mater. Sci. Eng. A* **2012**, *542*, 94–103. [[CrossRef](#)]
28. Carreño-Morelli, E.; Urreta, S.E.; Schaller, R. Mechanical spectroscopy of thermal stress relaxation at metal–ceramic interfaces in aluminium-based composites. *Acta Mater.* **2000**, *48*, 4725–4733. [[CrossRef](#)]
29. Walker, J.; Shadanbaz, S.; Woodfield, T.B.; Staiger, M.P.; Dias, G.J. Magnesium biomaterials for orthopedic application: A review from a biological perspective. *J. Biomed. Mater. Res. B Appl. Biomater.* **2014**, *102*, 1316–1331. [[CrossRef](#)] [[PubMed](#)]
30. Tsai, M.-H.; Chen, M.-S.; Lin, L.-H.; Lin, M.-H.; Wu, C.-Z.; Ou, K.-L.; Yu, C.-H. Effect of heat treatment on the microstructures and damping properties of biomedical Mg–Zr alloy. *J. Alloys Compd.* **2011**, *509*, 813–819. [[CrossRef](#)]
31. Wang, B.; Xu, D.; Dong, J.; Ke, W. Effect of corrosion product films on the in vitro degradation behavior of Mg-3% Al-1% Zn (in wt %) alloy in hank's solution. *J. Mater. Sci. Technol.* **2018**. [[CrossRef](#)]
32. Gupta, M.; Meenashisundaram, G.K. *Insight into Designing Biocompatible Magnesium Alloys and Composites: Processing, Mechanical and Corrosion Characteristics*; Springer: Berlin, Germany, 2015.

33. Cheng, M.; Chen, J.; Yan, H.; Su, B.; Yu, Z.; Xia, W.; Gong, X. Effects of minor Sr addition on microstructure, mechanical and bio-corrosion properties of the Mg–5Zn based alloy system. *J. Alloys Compd.* **2017**, *691*, 95–102. [[CrossRef](#)]
34. Taltavull, C.; Shi, Z.; Torres, B.; Rams, J.; Atrens, A. Influence of the chloride ion concentration on the corrosion of high-purity Mg, Ze41 and Az91 in buffered Hank's solution. *J. Mater. Sci. Mater. Med.* **2014**, *25*, 329–345. [[CrossRef](#)] [[PubMed](#)]
35. Meenashisundaram, G.K.; Nai, M.H.; Gupta, M. Effects of Ti and TiB<sub>2</sub> nanoparticulates on room temperature mechanical properties and in vitro degradation of pure Mg. In *Magnesium Technology 2015*; Manuel, M.V., Singh, A., Alderman, M., Neelameggham, N.R., Eds.; Springer International Publishing: Cham, Switzerland, 2016; pp. 413–418.
36. Ma, X.; Dong, L.; Wang, X. Microstructure, mechanical property and corrosion behavior of co-continuous β-TCP/MgCa composite manufactured by suction casting. *Mater. Des.* **2014**, *56*, 305–312. [[CrossRef](#)]
37. Wang, X.; Li, J.; Xie, M.; Qu, L.; Zhang, P.; Li, X. Structure, mechanical property and corrosion behaviors of (ha + β-TCP)/Mg–5Sn composite with interpenetrating networks. *Mater. Sci. Eng. C* **2015**, *56*, 386–392. [[CrossRef](#)] [[PubMed](#)]
38. Mostaed, E.; Hashempour, M.; Fabrizi, A.; Dellasega, D.; Bestetti, M.; Bonollo, F.; Vedani, M. Microstructure, texture evolution, mechanical properties and corrosion behavior of ecap processed ZK60 magnesium alloy for biodegradable applications. *J. Mech. Behav. Biomed. Mater.* **2014**, *37*, 307–322. [[CrossRef](#)] [[PubMed](#)]
39. Ahmadkhaniha, D.; Järvenpää, A.; Jaskari, M.; Sohi, M.H.; Zarei-Hanzaki, A.; Fedel, M.; Deflorian, F.; Karjalainen, L. Microstructural modification of pure Mg for improving mechanical and biocorrosion properties. *J. Mech. Behav. Biomed. Mater.* **2016**, *61*, 360–370. [[CrossRef](#)] [[PubMed](#)]
40. Pu, Z.; Song, G.-L.; Yang, S.; Outeiro, J.; Dillon, O., Jr.; Puleo, D.; Jawahir, I. Grain refined and basal textured surface produced by burnishing for improved corrosion performance of AZ31B Mg alloy. *Corros. Sci.* **2012**, *57*, 192–201. [[CrossRef](#)]
41. Zainal Abidin, N.I.; Atrens, A.D.; Martin, D.; Atrens, A. Corrosion of high purity Mg, Mg<sub>2</sub>Zn<sub>0.2</sub>Mn, ZE41 and AZ91 in Hank's solution at 37 °C. *Corros. Sci.* **2011**, *53*, 3542–3556. [[CrossRef](#)]
42. Geng, F.; Tan, L.; Jin, X.; Yang, J.; Yang, K. The preparation, cytocompatibility, and in vitro biodegradation study of pure β-TCP on magnesium. *J. Mater. Sci. Mater. Med.* **2009**, *20*, 1149–1157. [[CrossRef](#)] [[PubMed](#)]
43. Parande, G.; Manakari, V.; Kopparthy, S.D.S.; Gupta, M. Utilizing low-cost eggshell particles to enhance the mechanical response of Mg–2.5Zn magnesium alloy matrix. *Adv. Eng. Mater.* **2017**, *1700919*. [[CrossRef](#)]
44. Tun, K.; Zhang, Y.; Parande, G.; Manakari, V.; Gupta, M. Enhancing the hardness and compressive response of magnesium using complex composition alloy reinforcement. *Metals* **2018**, *8*, 276. [[CrossRef](#)]
45. Hermawan, H. Biodegradable metals: State of the art. In *Biodegradable Metals*; Springer: Berlin, Germany, 2012; pp. 13–22.



© 2018 by the authors. Licensee MDPI, Basel, Switzerland. This article is an open access article distributed under the terms and conditions of the Creative Commons Attribution (CC BY) license (<http://creativecommons.org/licenses/by/4.0/>).